A Fully Anlytical Model for Carbon Nanotube FETs including Quantum Capacitances and Electrostatics

Lan Wei[*], David J. Frank[^], Leland Chang[^], H.-S. Philip Wong[+]
[*]Microsystems Technology Laboratories, Massachusetts Institute of Technology, Cambridge, MA, 02139, USA.
[^] IBM T. J. Watson Research Center, Yorktown Heights, NY, 10598, USA
[+]Department of Electrical Engineering, Stanford University, Stanford, CA, 94305, USA.
lanwei@mit.edu, hspwong@stanford.edu

Abstract

In this paper, an analytical model of intrinsic carbon nanotube field effect transistors (CNFETs) is presented based on ballistic transport and careful analysis of the quantum capacitances, which requires neither iteration nor numeric integration. Essential physics, such as the drain-induced-barrier-lowing (DIBL) and quantum capacitances, are captured with a reasonable accuracy compared with numerical simulations. The model facilitates fast circuit simulation and system optimization.

1. Introduction

A hierarchy of models has been developed for carbon nanotube field effect transistor (CNFET), which is considered a potential candidate to replace or complement Si CMOS technology beyond the 11nm technology node [1, 2]. Significant benefits have been suggested in both transport and electrostatics [3, 4]. Different models abstract the device characteristics of CNFETs at different levels of abstraction, serving different purposes for different applications, including device design, optimization, and projection. Among these models, the non-equilibrium Green's function (NEGF) [5] approach starting from the first principle is rigorous in physics but is numerically intensive. Others [6, 7] are circuit-simulator compatible but require iterations for calculating the surface potential and quantum capacitance. Some computationally intensive applications, such as using the model within a system optimization loop [8], require a very simple analytical model to describe the intrinsic performance of CNFET, yet capture the essential physics. The compact models in [9, 10] are attempts for fast analytical solutions. However, these models all assume a re-distribution of channel carriers which fills the lower energy levels first, which is not valid when the channel length is comparable to or smaller than the carrier scattering mean free path, and inelastic scattering is negligible. Furthermore, capturing second order effects such as the drain-induced barrier lowing (DIBL) is necessary to correctly capture the short-channel device performance. In this paper, we develop a model that analytically includes source/drain coupling and accounts for the sources of the channel carriers when calculating the quantum capacitances in the case of ballistic transport with negligible scattering. Circuit simulation capability is demonstrated, and the model can be implemented into a system-level performance optimizer which enables chip-level design optimization and benchmarking of CNFETs [11].

2. Electrostatic Model

The MOSFET-like gate-all-around (GAA) structure (Fig. 1) is chosen for good gate electrostatic control [12, 13]. The CNTs (with diameter D) surrounded by dielectric layer (with thickness t_{ox} and dielectric constant k_{ox}) are patterned with a center-to-center pitch of s.

For ballistic transport, the channel surface potential (φ_{ch}), determines the drain current (I_d). For a low density of states material such as CNTs, φ_{ch} is determined by the capacitive network including both electrostatic and quantum capacitances (Fig. 2). In Fig. 2, C_{gc}, C_{fr_GS}, C_{fr_GD}, C_s and C_D are the electrostatic capacitances of gate-to-channel, gate-to-source, gate-to-drain, channel-to-source and channel-to-drain, respectively. C_{QTs}, C_{QTd}, C_{QRs}, and C_{QRd}, are quantum capacitances which will be discussed in Section 3. μ_S, μ_D and μ_G are the Fermi levels in the source, drain and gate, respectively. φ_S, φ_D, φ_G and φ_{ch} are the surface potentials in the source, drain, gate and channel respectively. Metal gate and degenerate

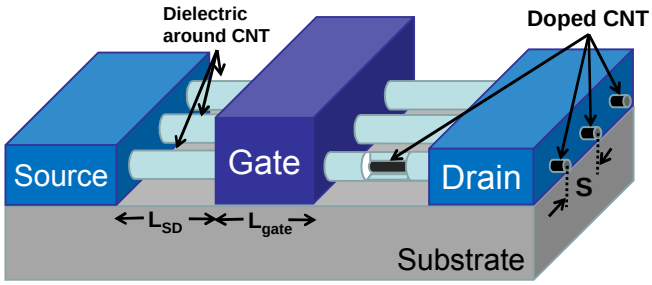

Fig 1 Schematics of MOSFET-like GAA CNFET

source/drain are assumed, while the Fermi level offset and surface potential in the source, drain and gate (not channel) are set as constants E_{FSD}, E_{FSD} and φ_{MS}. V_g and V_d are external applied voltages. R_s and R_D are the source/drain series resistances.

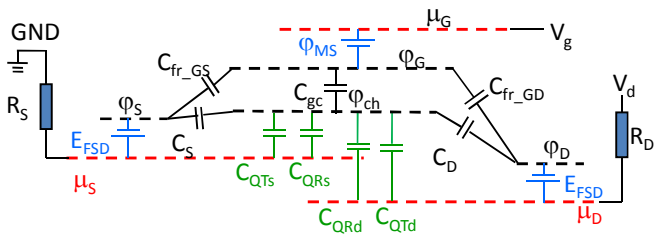

Fig 2 Electrostatic capacitances and quantum capacitances

It is important to include the electrostatic coupling from the source and drain to the channel for a short channel device, where second order effects, such as DIBL, introduces clear impact on I_d. Following the conformal mapping methodology [14], we model the source/drain coupling by introducing semi-empirical capacitances C_S and C_D (Eq. (1)-(4)). The ratio between C_S and C_D is empirically fitted to be 3.4, since the highest barrier moves toward the source side at large V_{ds}. Good agreement has been achieved between the model and numerical simulation (Fig. 3) in the practical range that we are interested in.

$$C_{gc} = \frac{2\pi k_{ox}\varepsilon_0 L_g}{\ln\left(\frac{r+t_{ox}}{r}\right)} \qquad (1)$$

$$a = 2 + b\left(\frac{0.5L_g}{t_{ox}}\right)^2, \quad b = 1.3 - 3.6\exp(-L_g/2.8r)$$

$$u = \arccos\left(\sqrt{0.5\cdot\left(a-\sqrt{a^2-4}\right)}\right) \qquad (2)$$

$$C_S + C_D = \left(\frac{\pi/2}{u} - 1\right)C_{gc} \qquad (3)$$

$$\frac{C_S}{C_D} = 3.4 \qquad (4)$$

3. Quantum Capacitance Model

When the energy level of the bottom of the conduction band (φ_{ch}) is pushed down by the electrostatic coupling under a positive gate bias, in the example of a n-type device, carriers populate in the channel area, which tends

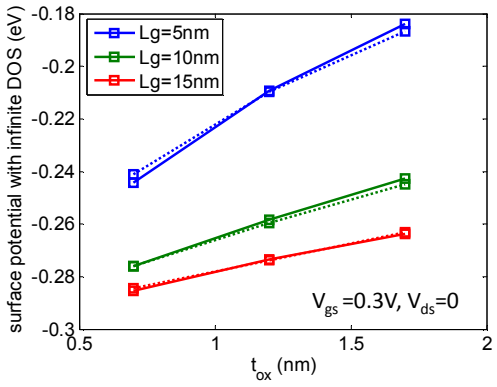

Fig 3 Comparison of the surface potential with only electrostatics between the numerical simulation (solid) and the analytical model (dashed).

to raise φ_{ch}. The impact of channel charges on φ_{ch} can be regarded as an equivalent quantum capacitance between the bottom of the conduction band and the Fermi energy (Fig. 2). For low DOS materials such as CNT, quantum capacitances can be comparable with intrinsic gate-to-channel electrostatic capacitances.

For devices with channel length comparable to or smaller than the mean free path, which is on the order of 10-100nm, we assume that these short-channel CNFETs operate at an ideal ballistic limit. Under this circumstance, both intra- and inter- subband inelastic scattering are negligible, and carriers do not redistribution in energy.

To solve the bias-dependent quantum capacitances in a low density of states material (such as CNT [15]) usually requires multiple iterations, which is undesirable when computational efficiency is critical. We carefully analyze which states are filled and which are empty for ideal ballistic transport, dividing the carriers into two types: (1) those that flow directly between source and drain ("transmitted carriers" with a population of Q_T), i.e., those above φ_{max}, and (2) those from the drain that are reflected back by the source barrier ("reflected carriers" with a population of Q_R) (Fig. 4). The channel carriers injected from the source are all transmitted carriers. They

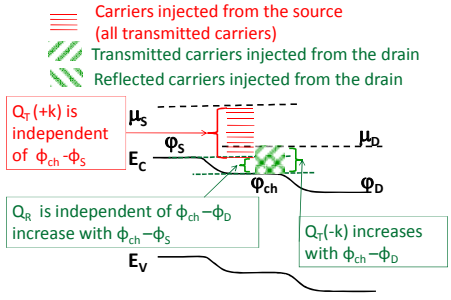

Fig 4 Band diagrams under selected bias conditions with reflected carriers

are directed injected into the channel and never change direction in k-space. A portion of $-k$ carriers in the drain are directly injected into the channel and then back-scattered in the $+k$ direction by the barrier at the source. Those $-k$ carriers are transmitted carriers while those $+k$ carriers are reflected carriers. Since both transmitted carriers and reflected carriers depend on both source and drain potential, there are two capacitance terms for each: C_{QTs}, C_{QTd}, C_{QRs}, C_{QRd}. C_{QTs} and C_{QTd} are the quantum capacitances related with transmitted carriers; while C_{QRs} and C_{QRd} are the quantum capacitances from reflected carriers. Empirically, φ_{ch} is roughly piecewise linear with V_g and V_d, as will be shown below in Fig. 6, hence we

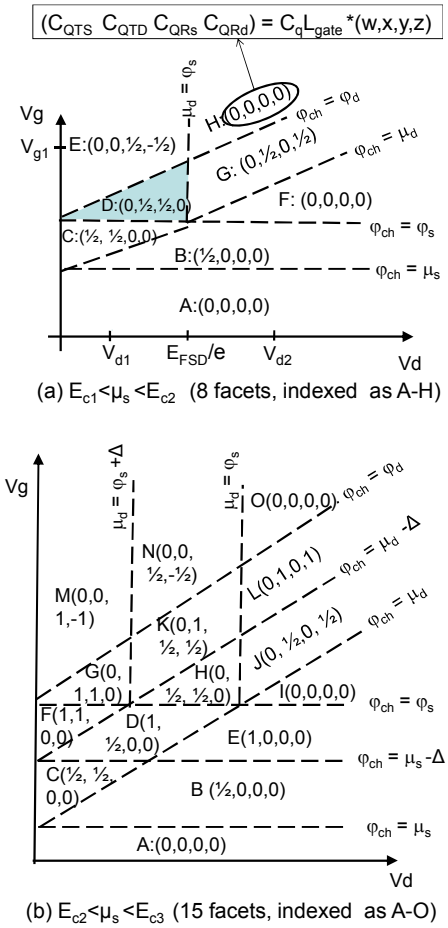

Fig 5 Visualization of bias-dependent quantum capacitances in V_g-V_d space The four quantum capacitance components are constants inside each facet. E_{ci} is the bandedge of the i^{th} subband. Assuming no inter-subband scattering, the source and drain can supply carriers from (a) only the 1st subband and (b) both 1st and 2nd subbands.

make a piecewise constant approximation for the quantum capacitances, where C_{QTs}, C_{QTd}, C_{QRs}, and C_{QRd} piecewise constant in each segment, in increments of ½C_q for carriers from a single side in a single subband. C_q is fitted to be 400aF/μm for CNTs as in Eq. (5).

$$\left.\begin{aligned} C_{QTs} &= \partial Q_T \big/ e\cdot\partial\mu_s,\ C_{QTd} = \partial Q_T \big/ e\cdot\partial\mu_d \\ C_{QRs} &= \partial Q_R \big/ e\cdot\partial\mu_s,\ C_{QRd} = \partial Q_R \big/ e\cdot\partial\mu_d \end{aligned}\right\} \Rightarrow \begin{cases} 0.5C_q, \text{ if positive at 0K} \\ 0, \text{ if 0 at 0K} \\ -0.5C_q, \text{ if negative at 0K} \end{cases} \quad (5)$$

$$\frac{\partial\varphi_{ch}}{\partial\mu_g} = \frac{C_{gc}}{C_{gc}+C_d+C_s+C_{Qtot}} \qquad \frac{\partial\varphi_{ch}}{\partial\mu_d} = \frac{C_d+C_{QTd}+C_{QRd}}{C_{gc}+C_d+C_s+C_{Qtot}} \quad (6)$$

where $C_{Qtot} = C_{QTd} + C_{QTs} + C_{QRs} + C_{QRd}$

The bias-dependent quantum capacitance components can be visualized using a multi-facetted V_g-V_d plane, with each facet of the V_g-V_d plane associating with a combination of constant C_{QTs}, C_{QTd}, C_{QRs} and C_{QRd} (Fig. 5). Facet D in (a) (shaded) corresponds to the band diagram in Fig 5. Following Eq. (6), φ_{ch} can be calculated as a piecewise linear function without iteration, assuming negligible scattering and minority carriers. Good agreement between our analytical model and numerical simulation (Fig. 6) validates our analysis and simplifications.

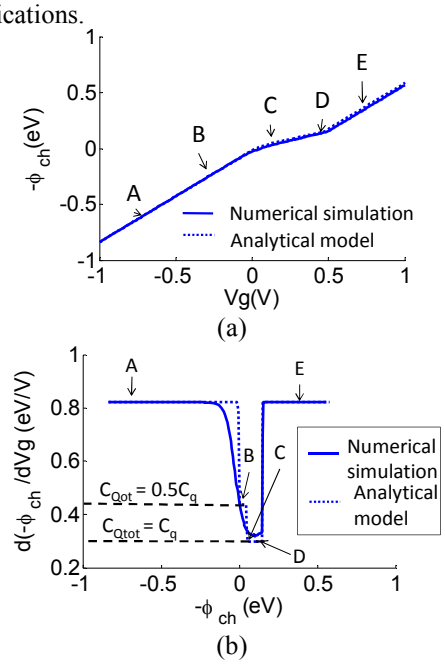

Fig 6 Comparison between simulation and our model of surface potential and its derivative over V_g of V_{d1} (=0.05V). The letters represent the facet index in Fig 5(a).

4. Transport Model

Using φ_{ch} and Eq. (7), a full IV model with no iteration or integration has been developed. T_i is the transmission coefficient of the i^{th} subband, which is set to

be 1 in the pure ballistic limit. DOS_i is the density of states of the i^{th} subband, which can be calculated as $\frac{1}{\pi}\Big/\frac{\partial E}{\partial k}$. v_i is the injected carrier velocity of the i^{th} subband, which is $\frac{1}{\hbar}\frac{\partial E}{\partial k}$. f_i is the Fermi-Dirac distribution of the i^{th} subband. F_0 is the zero-order Fermi integral. φ_{maxi}, μ_{Si}, and μ_{Di} are the highest barrier for the electrons, chemical potential at the source, chemical potential at the drain, for the i^{th} subband, respectively. The first two subbands are included. Again, no iterative method or numerical integration is involved. Sample IV curves are shown in Fig. 7. With the series resistance and parasitic capacitances model described in [6, 16], a complete CNFET model is obtained, whose capability of circuit simulation is demonstrated in Fig. 8.

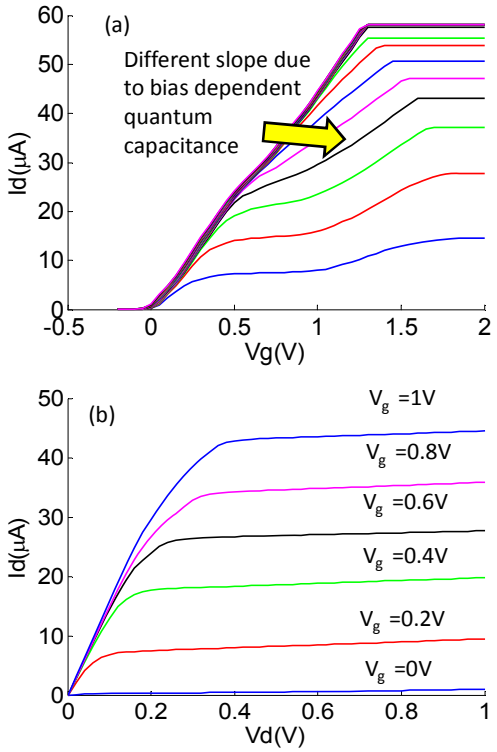

Fig 7 (a) I_d-V_g and (b) I_d-V_d curves for a CNFET with a (19, 0) CNT, L_{gate}=10nm, and EOT=1.5nm at 300K.

$$I_d = \sum_{i=1}^{2}\left(\begin{array}{l} 2e\cdot\left(\int_{\varphi_{\max i}}^{\infty} T_i\cdot DOS_i\cdot v_i\cdot f_i\cdot dE\right)_{source} \\ -2e\cdot\left(\int_{\varphi_{\max i}}^{\infty} T_i\cdot DOS_i\cdot v_i\cdot f_i\cdot dE\right)_{drain}\end{array}\right)$$
$$= \sum_{i=1}^{2}\left(\frac{4e}{h}\int_{\varphi_{\max i}}^{\infty} T_i\cdot f_i\cdot dE\Big|_{source} - \frac{4e}{h}\int_{\varphi_{\max}}^{\infty} T_i\cdot f_i\cdot dE\Big|_{drain}\right)$$
$$= \frac{4e}{h}\sum_{i=1}^{2}\left(F_0\left(-\frac{\varphi_{\max i}-\mu_{Si}}{kT}\right) - F_0\left(-\frac{\varphi_{\max i}-\mu_{Di}}{kT}\right)\right) \quad (7)$$

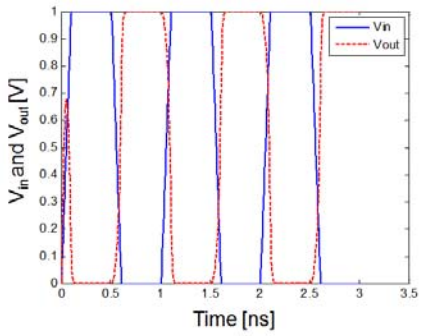

Fig 8 Input and output waveforms of a single stage inverter driving a 1fF load capacitance, calculated by the analytical model.

5. Conclusions

Without iteration or complex numerical integration, a simple analytical transport model for CNFETs is presented with an electrostatic capacitance model and a quantum capacitance model. This work provides a possible solution towards a computationally efficient compact model for CNFETs.

Acknowledgment

This work is partially supported by the Focus Center Research Program (FCRP), Center for Circuit and System Solutions (C2S2) and by IBM through the Stanford Center for Integrated Systems (CIS) Custom Research Fund. L.W. is additionally supported by the Stanford Graduate Fellowship. The authors would like to thank W. Haensch for his support.

Reference

[1] R. Chau, *et al.*, *T-ED,* vol. 4, pp. 153-158, 2005.

[2] P. Avouris, *et al.*, *Nat Nano,* vol. 2, pp. 605-615, 2007.

[3] J. Guo, *et al.*, *Applied Physics Letters,* vol. 80, pp. 3192-3194, 2002.

[4] Y. Ouyang, *et al.*, *Applied Physics Letters,* vol. 89, p. 203107, 2006.

[5] M. Lundstrom, J. Guo, *Nanoscale transistors: device physics, modeling and simulation*, Springer, 2006

[6] J. Deng and H. S. P. Wong, *T-ED*, vol. 54, pp. 3195-3205, 2007.

[7] B. C. Paul, *et al.*, *DAC,* pp. 717-722, 2006.

[8] D. Frank, *et al, IBM Journal of Research and Development*, vol. 50, pp. 419-431, 2006.

[9] A. Balijepalli, *et al, ISLPED,* pp. 2-7, 2007.

[10] T. J. Kazmierski, *et al.*, *T-Nano*, pp. 99-107, 2010.

[11] L. Wei, *et al.*, *IEDM*, paper 37.7, 2009.

[12] Z. Chen, *et al.*, *EDL,* vol. 29, pp. 183-185, 2008.

[13] J. P. Colinge et al, *IEDM*, 312-320, 1990.

[14] R. Plonsey and R. Collin, *Principles and Applications of Electromagnetic Fields*, p146-163. New York: McGraw-Hill, 1961.

[15] C. Dekker, *Phys. Today* 52, 22-28, 1999.

[16] L. Wei, J. Deng, H.-S. P. Wong, *IEDM,* p. 741, 2007.